


Quantized topological pumping of solitons in nonlinear photonics and ultracold atomic mixtures

Received: 3 January 2022

Nader Mostaan ^{1,2,3} , Fabian Grusdt^{1,2} & Nathan Goldman ³ 

Accepted: 20 September 2022


Published online: 11 October 2022

 Check for updates

Exploring the interplay between topological band structures and tunable nonlinearities has become possible with the development of synthetic lattice systems. In this emerging field of nonlinear topological physics, an experiment revealed the quantized motion of solitons in Thouless pumps and suggested that this phenomenon was dictated by the Chern number of the band from which solitons emanate. Here, we elucidate the origin of this nonlinear topological effect, by showing that the motion of solitons is established by the quantized displacement of the underlying Wannier functions. Our general theoretical approach, which fully clarifies the central role of the Chern number in solitonic pumps, provides a framework for describing the topological transport of nonlinear excitations in a broad class of physical systems. Exploiting this interdisciplinarity, we introduce an interaction-induced topological pump for ultracold atomic mixtures, where solitons of impurity atoms experience a quantized drift resulting from genuine interaction processes with their environment.

Quantized responses have been a central theme throughout the realm of topological physics, which was initiated with the discovery of the quantum Hall effects in two-dimensional electron gases^{1,2}. A wide variety of topological band structures have been revealed over the last decades, leading to the identification of various forms of quantized responses, from quantized Faraday and Kerr rotations in three-dimensional topological insulators³ to quantized circular dichroism⁴ and topological Bloch oscillations^{5,6} in two-dimensional ultracold atomic gases. An emblematic and minimal instance of quantized topological transport concerns the adiabatic motion of a quantum particle moving in a slowly-varying periodic potential, an effect known as the Thouless pump⁷. In this setting, the center-of-mass motion is quantized according to the Chern number of the underlying band structure, as defined over a hybrid momentum-time space⁸. The realization of synthetic lattice systems has allowed for the experimental implementation of Thouless pumps and for the observation of the related quantized motion, in both photonics^{9–14} and ultracold gases setups^{15,16}.

Interestingly, synthetic topological systems^{17,18} can operate beyond the linear regime of the Schrödinger equation, hence opening the door to nonlinear topological physics¹⁹. In this emerging framework, a central topic concerns the possible interplay between nonlinear excitations, known as solitons, and the underlying topological band structure^{20–31}. Interestingly, exact correspondences between topological indices and nonlinear modes have been identified in mechanical systems³² and for the Korteweg-de-Vries equation of fluid dynamics³³, hence allowing for a formal topological classification of nonlinear excitations in certain special cases. In the context of nonlinear topological photonics, a recent experimental study reported on the quantized motion of solitons in a lattice system undergoing a Thouless pump sequence³⁴. Despite the presence of considerable nonlinearity, these observations suggest that the quantization of the solitons displacement is dictated by the Chern numbers of the underlying band structure. This nonlinear topological effect is particularly intriguing: On the one hand, the soliton is associated with a non-uniform occupation of a Bloch band, hence violating the standard

¹Department of Physics and Arnold Sommerfeld Center for Theoretical Physics (ASC), Ludwig-Maximilians-Universität München, Theresienstr. 37, D-80333 München, Germany. ²Munich Center for Quantum Science and Technology (MCQST), Schellingstr. 4, D-80799 München, Germany. ³CENOLI, Université Libre de Bruxelles, CP 231, Campus Plaine, B-1050 Brussels, Belgium.  e-mail: Nader.Mostaan@physik.uni-muenchen.de; ngoldman@ulb.ac.be

condition for quantized motion in conventional (linear) Thouless pumps^{7,8}. On the other hand, the nonlinearity prevents the dispersive evolution of a localized wave packet through the formation of a soliton. As already pointed out in ref. 34, these facts highlight the crucial role of nonlinearities in this emerging context of soliton Thouless pumps.

In this work, we elucidate and explore the quantized transport of solitons in nonlinear topological Thouless pumps. Inspired by the experiment of ref. 34, we address this topic by considering a general class of one-dimensional systems described by the discrete nonlinear Schrödinger equation (DNLS)^{35,36}. Following ref. 37, we represent the solitons in terms of maximally localized Wannier functions of the corresponding Bloch band from which the soliton bifurcates. In the so obtained Wannier representation, the adiabatic motion of the soliton can be deduced from an ordinary (scalar) DNLS; from this, we show that the quantized motion of the soliton is directly related to the quantized displacement of Wannier functions upon pumping, which is known to be set by the Chern number of the band^{15,38,39}. This general approach allows us to mathematically demonstrate the topological nature of nonlinear Thouless pumps, by relating the quantized motion of solitons to the Chern number of the underlying Bloch band. More generally, these developments introduce a theoretical framework by which a broad class of nonlinear topological phenomena can be formulated in terms of topological band indices. We then broaden the scope by applying this nonlinear topological framework to the realm of quantum gases. By considering an instructive mapping to a Bose-Bose atomic mixture on a lattice^{40–42}, which encompasses the aforementioned DNLS as its semiclassical limit, we identify a scenario by which a topological pump emerges from inter-particle interaction processes: a soliton of impurity atoms is dragged by the driven majority atoms, hence leading to interaction-induced topological transport.

Results

Topological pumps of solitons: General theory

The theoretical description of soliton pumping relies on the topological character of Wannier functions, namely, the displacement of Wannier centers per pump cycle by the Chern number of the associated Bloch band, see Fig. 1a. An intuitive reason for soliton pumping then is solitons are dragged by Wannier functions, resulting in their topologically quantized motion, see Fig. 1b. Interestingly, nonlinearities can induce this drag effect in topologically trivial systems. To demonstrate this effect, we consider a 1D atomic Bose-Bose mixture in a species-selective optical lattice, where the majority (minority) atoms experience a topological (trivial) lattice. We show that a soliton of minority atoms undergoes quantized displacement by activating a Thouless pump sequence for the majority atoms; see Fig. 1c. In the following, we elaborate on the theoretical description of soliton motion in nonlinear Thouless pumps and the interaction-induced topological pumps for atomic mixtures.

Our theoretical framework concerns a generic class of lattice models governed by the DNLS,

$$i\partial_t \phi_{i,\alpha} = \sum_{j,\beta} H_{ij}^{\alpha\beta}(t) \phi_{j,\beta} - g |\phi_{i,\alpha}|^2 \phi_{i,\alpha}, \quad (1)$$

where the field $\phi_{i,\alpha}$ is defined at the lattice site α of the i th unit cell; $H(t)$ is a time-dependent Hamiltonian matrix, which includes a Thouless pump sequence^{7,38}; and $g > 0$ is the (onsite) nonlinearity strength. Equation (1) preserves the norm of the field, which we set to $\sum_{\alpha,i} |\phi_{i,\alpha}|^2 = 1$, without loss of generality.

An illustrative model, used below to validate the general theory, is provided by the two-band Rice-Mele model¹⁵: a 1D chain with alternating couplings $J_{1,2}(t)$ and staggered potential $\pm\Delta(t)$

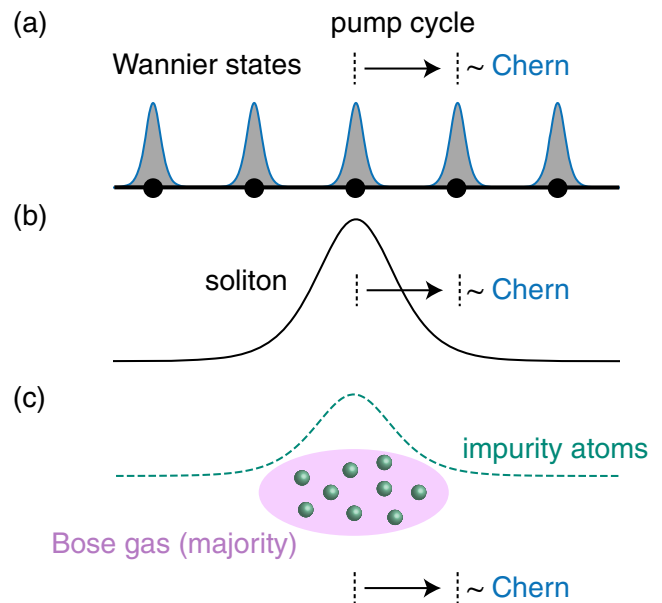


Fig. 1 | Schematics of the soliton pumping mechanism and nonlinearity-induced pumping in ultracold mixtures. **a** In a Thouless pump, the Wannier functions perform a quantized drift established by the Chern number of the corresponding band. **b** In a nonlinear setting, the motion of a soliton follows the quantized Wannier drift. **c** In a Bose-Bose atomic mixture, quantized pumping can be induced by interactions: a soliton of impurity atoms is dragged by the driven majority atoms, leading to interaction-induced topological transport.

(Methods). Considering the *nonlinear* Rice-Mele model, Eq. (1) takes the more explicit form

$$\begin{aligned} i\partial_t \phi_{i,1} &= J_1(t) \phi_{i,2} + J_2(t) \phi_{i-1,2} + \Delta(t) \phi_{i,1} - g |\phi_{i,1}|^2 \phi_{i,1}, \\ i\partial_t \phi_{i,2} &= J_1(t) \phi_{i,1} + J_2(t) \phi_{i+1,1} - \Delta(t) \phi_{i,2} - g |\phi_{i,2}|^2 \phi_{i,2}. \end{aligned} \quad (2)$$

Here, the Thouless pump cycle corresponds to a loop in the parameter space spanned by $(J_2 - J_1)$ and Δ , which encircles the origin ($J_1 = J_2, \Delta = 0$); see Methods. When $g = 0$, the Bloch bands defined in momentum-time space are associated with a Chern number $C = \pm 1$. This topological invariant is known to determine the quantized displacement for a filled band upon each cycle of the pump³⁸.

Our analysis starts by studying the adiabatic evolution associated to the general Eq. (1), which is characterized by the period of the pump T (exceeding all other time scales). To simplify notations, we use the multi-index $\mathbf{i} = (i, \alpha)$ and write $H_{\mathbf{ij}} \equiv H_{\mathbf{ij}}^{\alpha\beta}(t)$. Introducing the *adiabatic time* $s = t/T$, Eq. (1) takes the form $i\varepsilon \partial_s \phi_{\mathbf{i}} = \sum_{\mathbf{j}} H_{\mathbf{ij}}(s) \phi_{\mathbf{j}} - g |\phi_{\mathbf{i}}|^2 \phi_{\mathbf{i}}$, where $\varepsilon = 1/T$. The solutions to the adiabatic DNLS can be well approximated by stationary states of the form $\phi_{\mathbf{i}} \propto e^{-i\theta_s} \varphi_{\mathbf{i}}$, where θ_s is a time-dependent phase factor and $\varphi_{\mathbf{i}}$ is an instantaneous solution to the stationary nonlinear Schrödinger equation (see Methods and refs. 43, 44)

$$\mu_s \varphi_{\mathbf{i}} = \sum_{\mathbf{j}} H_{\mathbf{ij}}(s) \varphi_{\mathbf{j}} - g |\varphi_{\mathbf{i}}|^2 \varphi_{\mathbf{i}}, \quad (3)$$

where the instantaneous eigenvalue μ_s explicitly depends on the adiabatic time s .

Equation (3) admits (bright) solitons as stationary state solutions, which are stable localized structures in the bulk. For sufficiently weak nonlinearity, solitons predominantly occupy the band from which they bifurcate⁴⁵, while increasing nonlinearity leads to band mixing. In real space, solitons are immobile without external forcing, and are degenerate modulo a lattice translation set by the translational

symmetry of the system. By adiabatically changing the Hamiltonian $H_{\text{eff}}(s)$, a single soliton undergoes smooth deformation, and after one period, it is mapped to the manifold of initial solutions, implying translation by an integer multiple of the unit cell. The observations of ref. 34 suggest that solitons bifurcating from a single Bloch band undergo a quantized displacement dictated by the Chern number of the band⁷ over each pump cycle. Demonstrating this intriguing relation between the transport of nonlinear excitations and topological band indices is at the core of the present work.

To elucidate the topological nature of nonlinear pumps, we follow ref. 37 and represent the solitons of Eq. (3) in the basis of maximally localized Wannier states,

$$\varphi_i = \sum_n \varphi_i^{(n)}, \quad \varphi_i^{(n)} = \sum_l a_l^{(n)} w_i^{(n)}(l), \quad (4)$$

where the superscript n denotes the occupied band; the index l labels the unit cell on which the Wannier state is localized; and all dependence on the adiabatic time s is henceforth implicit. The coefficients $a_l^{(n)}$ obey the analogue of Eq. (3) in the Wannier representation (Methods)

$$\begin{aligned} \mu_s a_l^{(n)} = & \sum_{l_1} \omega_{l-l_1}^{(n)} a_{l_1}^{(n)} \\ & - g \sum_{n_1, n_2, n_3} \sum_{l_1, l_2, l_3} W_{l-l_1}^{(n)} a_{l_1}^{(n_1)*} a_{l_2}^{(n_2)} a_{l_3}^{(n_3)}, \end{aligned} \quad (5)$$

where $\omega_l^{(n)} = 1/N \sum_{k=0}^{N-1} \exp(i(2\pi/N)kl) \epsilon_k^{(n)}$ is the Fourier transform of the n th Bloch band $\epsilon_k^{(n)}$ associated with $H_{\text{eff}}(s)$; N is the number of unit cells; $\underline{n} = (n, n_1, n_2, n_3)$, $\underline{l} = (l, l_1, l_2, l_3)$; and $W_{\underline{l}}^{(n)}$ are the following Wannier overlaps

$$W_{\underline{l}}^{(n)} = \sum_j w_j^{(n)*}(l) w_j^{(n_1)*}(l_1) w_j^{(n_2)}(l_2) w_j^{(n_3)}(l_3). \quad (6)$$

The Wannier states of a Bloch band are not unique, as they depend on the gauge choice for the Bloch functions⁴⁶. Nevertheless, a unique set of maximally localized Wannier functions is provided by the eigenstates of the position operator’s projection onto the associated band. Since such Wannier functions are exponentially localized, the contribution to the Wannier overlaps in Eq. (6) from Wannier functions corresponding to different unit cells are negligible. The Wannier overlaps can thus be simplified as $W_{\underline{l}}^{(n)} = W^{(n)} \delta_{ll_1} \delta_{l_1 l_2} \delta_{l_2 l_3}$, where $W^{(n)} = \sum_j w_j^{(n)*}(l) w_j^{(n_1)*}(l) w_j^{(n_2)}(l) w_j^{(n_3)}(l)$; we point out that $W^{(n)}$ does not depend on the index l , because of translational invariance.

Moreover, in the regime of weak nonlinearity, the initial state soliton occupies a single band^{34,37,47}, which allows us to neglect inter-band contributions to Eq. (5). We note that this simplification holds throughout the evolution of the pump, during which the soliton adiabatically follows the same band.

Under those realistic assumptions, the Wannier representation of the DNLS reduces to the form

$$\mu_s a_l^{(n)} = \sum_{l_1} \omega_{l-l_1}^{(n)} a_{l_1}^{(n)} - g W^{(n)} |a_l^{(n)}|^2 a_l^{(n)}, \quad (7)$$

where $W^{(n)} = \sum_j |w_j^{(n)}(l)|^4$. Equation (7) has the form of a scalar DNLS on a simple lattice with one degree of freedom per unit cell labeled by Wannier indices l , with hopping terms involving nearest and beyond-nearest neighbors. The properties of such scalar DNLS are well established^{36,48,49}; Equation (7) admits inter-site solitons, with maxima on two adjacent sites, and on-site solitons, with their maximum on a single site. The inter-site solitons are known to be unstable against small perturbations, we thus restrict ourselves to the stable on-site solitons. Crucially, on-site solitons are always peaked around a single

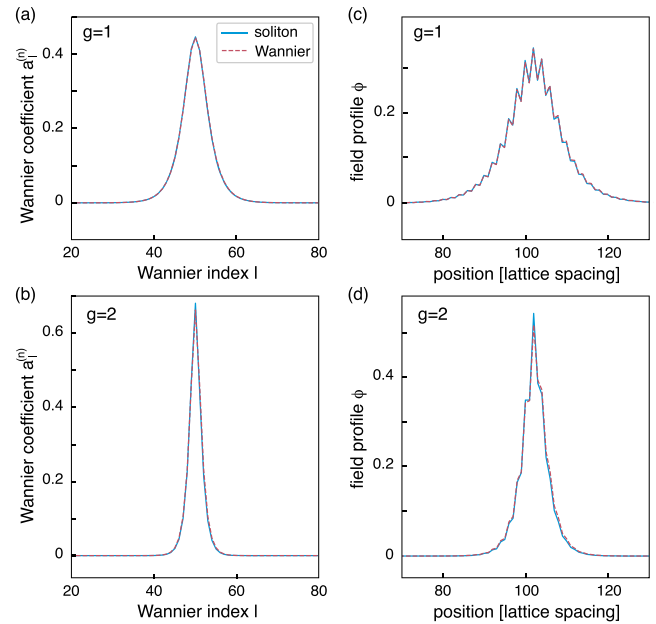


Fig. 2 | Numerical validation of the simplified theoretical scheme. **a, b** Wannier representation of a soliton in the lowest band ($n=0$) of the nonlinear Rice-Mele model (blue solid line), compared with the soliton obtained from the simplified DNLS Eq. (7) (dashed red line), for $g=J_0$ and $g=2J_0$ and time $s=0.12$. Here, J_0 is a characteristic hopping strength (Methods). Note how increasing the nonlinearity further localizes the soliton. **c, d** Same comparison in real space.

site (l) throughout the pumping cycle, as there is a finite energy (Peierls-Naborro) barrier for delocalization^{36,49}. Interestingly, the Peierls-Naborro barrier plays a role analogous to the “gap condition” of conventional topological physics, by forbidding transitions to other stable states during the adiabatic time evolution (Methods). This observation suggests that solitons are dragged by Wannier states upon pumping, hence exhibiting a quantized displacement in real space established by the Chern number^{15,38,39}; see Fig. 1a, b.

To firmly prove the topological nature of the nonlinear Thouless pump, we evaluate the solitons center-of-mass displacement after one period $s=1$ (Methods)

$$\begin{aligned} \Delta \langle \varphi^{(n)}, X \varphi^{(n)} \rangle = & \Delta \langle w^{(n)}(0), X w^{(n)}(0) \rangle \\ & + \Delta \sum_{l \neq l'} a_l^{(n)*} a_{l'}^{(n)} \langle w^{(n)}(l'), X w^{(n)}(l) \rangle, \end{aligned} \quad (8)$$

where X is the position operator of the lattice; $\langle f, g \rangle \equiv \sum_i f_i^* g_i$ is the inner product of fields on the lattice; and $\Delta(\cdot) \equiv (\cdot)_{s=1} - (\cdot)_{s=0}$. The first term in Eq. (8) reflects the displacement of Wannier functions upon one pump cycle, which is known to correspond to the Chern number of the band^{15,38,39}; the additional terms displayed on the second line are possible corrections due to the finite overlap of different Wannier states. Importantly, we find that these small interference effects are periodic in time (Methods), such that these correction terms in Eq. (8) do not contribute to the solitons center-of-mass displacement over a pump cycle. Altogether, this completes the proof: the displacement of solitons is indeed quantized according to the Chern number of the band from which they emanate.

Numerical validation

We now demonstrate the validity of our assumptions by solving the nonlinear Rice-Mele model [Eq. (2)]. In Fig. 2a, b, we compare the on-site soliton solution of the simplified Eq. (7), which emerges from the lowest band, with the Wannier representation of the exact soliton obtained by

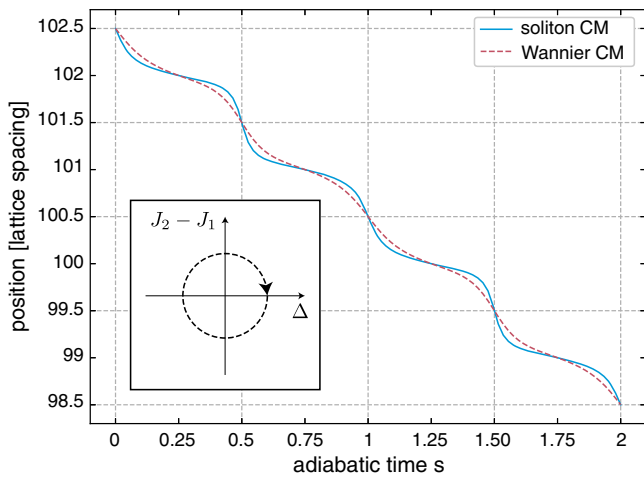


Fig. 3 | Comparison of soliton and Wannier function center-of-mass displacement. Adiabatic evolution of the soliton’s center-of-mass (CM) during two full pump cycles (inset), as obtained by solving Eq. (3) on the Rice-Mele lattice with $g = J_0$, and selecting a soliton in the lowest band. This is compared to the evolution of the center-of-mass of the Wannier function with largest contribution to the soliton’s expansion [Eq. (4)]. For clarity, the Wannier functions are relabeled during the pump cycle such that their center-of-mass follows a contiguous path instead of winding around a unit cell. The quantized displacement is set by the Chern number $C = -1$ of the occupied band.

solving the full DNLS in Eq. (3). We then perform a similar comparison in real space, by convolving the soliton of Eq. (7) with the corresponding Wannier states, and by comparing this result to the exact soliton of the original nonlinear Rice-Mele model; see Fig. 2c, d. The perfect agreement validates the description of the soliton in Wannier representation using the ordinary nonlinear Schrödinger Eq. (7).

We depict the motion of the exact soliton in Fig. 3, as obtained by solving Eq. (3) over two pump cycles $s \in [0, 2]$, and we compare this trajectory with the drift of its underlying Wannier function, i.e., the Wannier state that contributes the most to the expansion (4). In order to obtain a contiguous path for the Wannier center, we relabeled the Wannier functions whenever the Wannier centers met discontinuities; this smoothing corresponds to a singular gauge transformation of the corresponding Bloch states, and has no physical implication. Figure 3 indicates that the trajectories of the soliton and Wannier center differ at intermediate times ($s \neq \text{integer}$), which we attribute to the aforementioned interference effects involving different Wannier states (Methods); however, in agreement with our theoretical predictions, this deviation remains small and time-periodic over the whole pump cycle, and does not introduce any (integer) correction to the quantized center-of-mass displacement.

An interaction-induced topological pump for ultracold atomic mixtures

The theoretical framework presented in this work is based on the general DNLS in Eq. (1), and hence, it applies to a broad range of nonlinear lattice systems. In particular, this equation corresponds to the Gross-Pitaevskii equation describing a weakly-interacting Bose gas evolving on a moving lattice potential. In this section, we propose to go beyond the paradigm of nonlinear pumps for single-component bosonic systems, by introducing a mapping to an imbalanced Bose-Bose atomic mixture, which encompasses the DNLS in Eq. (1) as its semi-classical limit (within the Thomas-Fermi approximation). As we explain below, this original approach reveals an interaction-induced topological pump, where solitons of impurity atoms undergo a quantized drift resulting from genuine interaction processes with their environment.

We start from a microscopic theory for an imbalanced Bose-Bose atomic mixture on a 1D lattice⁴², as described by the second-quantized

Hamiltonian

$$\begin{aligned} \hat{H} = & \sum_{\langle i,j \rangle} \hat{\phi}_i^\dagger H_{ij}^{(\phi)} \hat{\phi}_j + \sum_i \frac{U_{\phi\phi}}{2} \hat{\phi}_i^\dagger \hat{\phi}_i \hat{\phi}_i \hat{\phi}_i \\ & + \sum_{\langle i,j \rangle} \hat{\sigma}_i^\dagger H_{ij}^{(\sigma)} \hat{\sigma}_j + \sum_i \frac{U_{\sigma\sigma}}{2} \hat{\sigma}_i^\dagger \hat{\sigma}_i \hat{\sigma}_i \hat{\sigma}_i \\ & + \sum_i U_{\phi\sigma} \hat{\phi}_i^\dagger \hat{\phi}_i \hat{\sigma}_i^\dagger \hat{\sigma}_i, \end{aligned} \quad (9)$$

where $\hat{\phi}_i$ and $\hat{\sigma}_i$ are bosonic field operators on the lattice; note that we use the same conventions for indices $\mathbf{i} = (i, \alpha)$ as before. Specifically, the first line describes single-body processes (i.e., nearest-neighbor hopping and onsite potentials) and intra-species contact interaction processes for the majority atoms, which are described by the field operator $\hat{\phi}_i$; the second line describes single-body processes and intra-species contact interactions for impurity atoms, represented by the field operator $\hat{\sigma}_i$; and the third line describes inter-species interaction processes. We assume that the intra-species interaction strengths are both repulsive, ($U_{\sigma\sigma}, U_{\phi\phi} > 0$), whereas the inter-species interaction strength is attractive ($U_{\phi\sigma} < 0$).

In the semi-classical limit, where quantum fluctuations are suppressed for both species, this Bose-Bose mixture setting is well described by two coupled nonlinear Schrödinger equations (Methods and ref. 42)

$$\begin{aligned} (\omega_0 + \mu_\phi) \phi_i - \sum_j H_{ij}^{(\phi)} \phi_j - (g_{\phi\phi} |\phi_i|^2 + g_{\phi\sigma} |\sigma_i|^2) \phi_i &= 0, \\ (\omega_0 + \mu_\sigma) \sigma_i - \sum_j H_{ij}^{(\sigma)} \sigma_j - (g_{\phi\sigma} |\phi_i|^2 + g_{\sigma\sigma} |\sigma_i|^2) \sigma_i &= 0, \end{aligned} \quad (10)$$

where ϕ_i and σ_i denote classical fields satisfying the constraints $\sum_i |\phi_i|^2 = N_\phi / (N_\phi + N_\sigma)$ and $\sum_i |\sigma_i|^2 = N_\sigma / (N_\phi + N_\sigma)$, with N_ϕ and N_σ the particle number of majority and impurity species, respectively; the interaction parameters are defined as $g_{\alpha\beta} = U_{\alpha\beta} (N_\phi + N_\sigma)$, with $\alpha, \beta = (\phi, \sigma)$; $\mu_{\phi,\sigma}$ denote the chemical potentials; and ω_0 is the eigenvalue of the nonlinear Eqs. (10).

Considering the case of heavy impurities, we neglect their kinetic energy contributions ($H_{ij}^{(\sigma)}$) to Eq. (10), the so-called Thomas-Fermi approximation. In this regime, one can relate the impurity mean-field profile to the majority profile as

$$|\sigma_i|^2 = - (g_{\phi\sigma} / g_{\sigma\sigma}) |\phi_i|^2, \quad (11)$$

and Eq. (10) simplifies to the DNLS (Methods)

$$(\omega_0 + \mu_\phi) \phi_i = \left(\sum_j H_{ij}^{(\phi)} - u_i^{\text{MF}} \right) \phi_i, \quad u_i^{\text{MF}} = g |\phi_i|^2, \quad (12)$$

where $g = -g_{\phi\phi} + g_{\phi\sigma}^2 / g_{\sigma\sigma}$. Interestingly, Eq. (12) is formally equivalent to the DNLS in Eq. (3): the majority atoms described by the field ϕ_i can form a soliton and undergo a quantized motion upon driving a Thouless pump sequence in the corresponding lattice Hamiltonian, i.e., $H_{ij}^{(\phi)}(s)$. Importantly, according to Eq. (11), the impurity atoms also form a soliton and undergo a quantized motion: the impurities exhibit topological pumping from genuine interaction processes with the majority atoms. In particular, this interaction-induced topological pumping occurs even when the lattice felt by the impurities $H_{ij}^{(\sigma)}$ is associated with a trivial (non-topological) band structure. This intriguing phenomenon, which could be implemented in ultracold atomic mixtures in optical lattices⁴⁰⁻⁴², is reminiscent of topological polarons⁵⁰⁻⁵⁵, in the sense that impurities inherit the topological properties of their environment through genuine interaction processes.

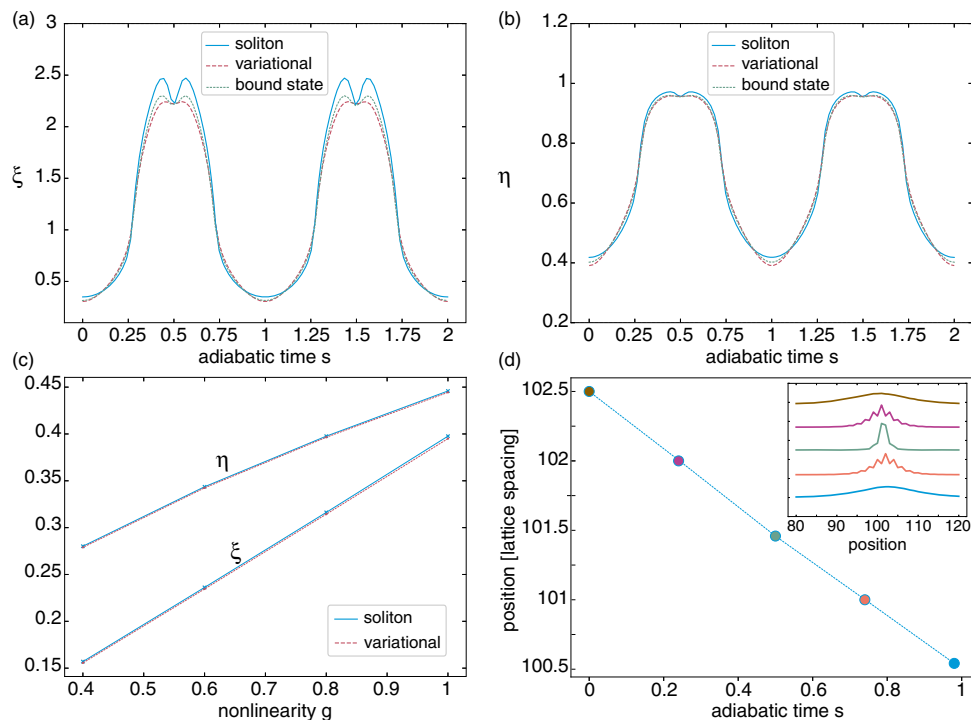


Fig. 4 | Characterizing soliton evolution during two pump cycles. **a** Evolution of the soliton’s width ξ in Wannier space over two pump cycles, as obtained by fitting the numerical solution of Eq. (3) with a sech function (blue solid line). This is compared to the width of the variational-ansatz solution (dashed red line), and to that of the bound-state solution (green dotted line); here $g = J_0$. **b** Same for the

amplitude of the soliton η . **c** Amplitude and width of the exact (solid blue line) and variational-ansatz (dashed red line) solutions as a function of g , at time $s = 0.12$. **d** Center-of-mass displacement of the calculated bound state over one pump cycle. The inset shows the corresponding bound state profiles. The quantized motion is dictated by the Chern number $C = -1$; compare with Fig. 3.

We first analyze this interaction-induced topological effect by considering the Thomas-Fermi approximation. It appears from Eq. (12) that u^{MF} acts as an effective potential for the majority atoms; a soliton then emerges as the bound state of the impurity field. In the context of highly-imbalanced mixtures with strong impurity-majority coupling, i.e., in the strong-coupling Bose polaron regime, it is customary to assume a variational ansatz describing the profile of the impurity and majority fields⁵⁶; the majority field is then found as the bound state of the impurity potential u^{MF} using the first relation in Eq. (12). Here, the variational problem for obtaining u^{MF} reduces to one for ϕ , because of the constraint $u^{\text{MF}} = g|\phi|^2$. As before, we express ϕ in the Wannier basis, and the variational problem is then solved simultaneously for both u^{MF} and ϕ using the ansatz $a_l = \eta \text{sech}(\xi(l - l_0))$ for the Wannier coefficients of ϕ . The bound state of the resulting impurity potential $u^{\text{MF}} = g|\phi|^2$ then corresponds to the soliton (Methods).

Figure 4 a, b show the adiabatic evolution of the amplitude η and width ξ of the variational solution $a_l = \eta \text{sech}(\xi(l - l_0))$ used for the Wannier coefficients of ϕ . We compare these results with the amplitude and width extracted from the bound-state solution associated with the impurity potential $u_{\text{MF}} = g|\phi|^2$, as well as to those extracted from the exact soliton of Eq. (3) expressed in Wannier representation. We also show the dependence of these parameters on the nonlinearity g in Fig. 4c, for both the exact soliton and the variational solution. These results validate our variational approach, as well as the bound-state picture of our soliton.

The minimum-energy solutions obtained from the variational ansatz are realized for integer values of the Wannier index l_0 , and thus correspond to stable on-site solitons. Moreover, this Wannier index l_0 remains constant over a pump cycle. Hence, this again suggests that the real-space motion of the soliton should follow the quantized Wannier drift, as established by the Chern number. This is verified in Fig. 4d, where the center-of-mass displacement of the calculated bound state is shown to be quantized over a pump cycle (compare with Fig. 3).

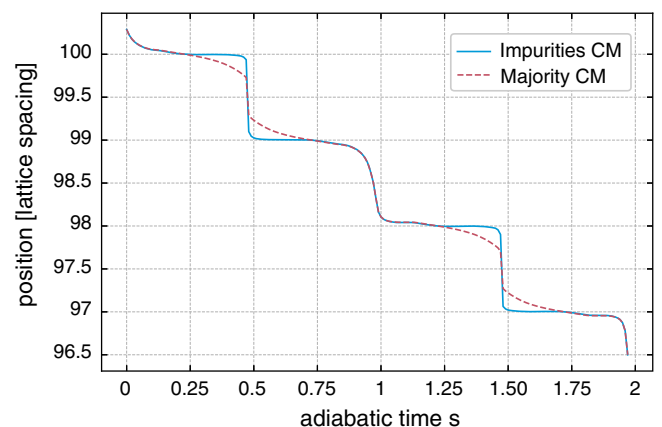


Fig. 5 | Nonlinearity-induced topological pumping in a Bose-Bose mixture. Center-of-mass (CM) trajectories of both species in a Bose-Bose mixture. Here, the interaction strengths are set as $g_{\phi\phi} \approx 0.226J_0$, $g_{\phi\sigma} \approx -11.32J_0$ and $g_{\sigma\sigma} \approx 2.26J_0$. The majority atoms undergo the pumping sequence as in Fig. 3, while impurities feel a trivial sequence (Methods). Impurity atoms undergo quantized transport through interactions with their environment.

In order to demonstrate the validity of our results, in particular, the robustness of the interaction-induced topological pump away from the Thomas-Fermi limit, we solve Eq. (10) numerically for a mass-balanced mixture, thus including the effects of the impurities’ kinetic energy. We again use the Rice-Mele model, but consider two different pump sequences for the majority and impurity species: the majority feels the same (topological) pump sequence as in Fig. 3, while we apply a trivial sequence for the impurity species. We obtain the steady state solution of Eq. (10) over two pump cycles, where the majority particles predominantly occupy the lowest Bloch band. The corresponding

trajectories of the CM of both species are depicted in Fig. 5, where the impurity CM is shown to be dragged by the majority particles. While the exact form of the CM trajectories depend on the details of the model and pumping sequence, the CM displacement after one pump cycle is dictated by the Chern number of the topological band occupied by the majority species ($C = -1$ in this case). Although the impurity atoms experience a topologically trivial lattice, they are shown to undergo topological pumping through genuine interaction effects with their environment.

Implementation in ultracold atoms

The interaction-induced topological pump introduced above could be experimentally implemented in ultracold atomic gases involving two bosonic species. In fact, the parameters values incorporated in our numerical simulations of Eq. (10), and displayed in Fig. 5, are compatible with an experimental realization based on bosonic ${}^7\text{Li} - {}^7\text{Li}$ mixtures, with two different hyperfine states of ${}^7\text{Li}$ as “majority” and “impurity” atoms; we note that the formation of solitons in Lithium gases was previously investigated, both theoretically and experimentally^{57,58}. Following ref. 59, the scattering lengths between atoms in state ($F=1, m_F=1$)–“impurity” atoms–and ($F=1, m_F=0$)–“majority” atoms–can be set to $a_{\phi\phi} \approx 0.154 a_0$, $a_{\phi\sigma} \approx -7.57 a_0$, $a_{\sigma\sigma} \approx 1.514 a_0$, at a magnetic field $B \approx 575 G$, where a_0 is the Bohr radius ($a_0 = 0.0529 \text{ nm}$); we note that these scattering lengths are highly tunable thanks to a broad Feshbach resonance. As further discussed below, this configuration is compatible with the interaction parameters ($g_{\phi\phi}$, $g_{\sigma\sigma}$, $g_{\phi\sigma}$) used in our numerics.

The lattice structure and pump sequence can be designed within a time-dependent optical lattice. For instance, following ref. 16, the atoms can be loaded in a potential landscape comprised of two superimposed optical lattices, with a long-wavelength lattice ($\lambda_l = 1064 \text{ nm}$) and a shorter lattice ($\lambda_s = \lambda_l/2$), with different amplitudes ($V_l = 3.0 E_R$ and $V_s = 1.0 E_R$, with $E_R = \hbar^2/(2m\lambda_l^2)$ the recoil energy of the long lattice). Such an optical lattice potential takes the form $V(x, \phi) = -V_l \cos^2(2\pi x/\lambda_l - \phi) - V_s \cos^2(2\pi x/\lambda_s)$, and it implements the Rice-Mele lattice considered in our numerics: the Thouless pump sequence is simply realized by sweeping the phase ϕ from 0 to 2π . The relevant parameters of the Rice-Mele model can be extracted from a tight-binding analysis of the optical lattice potential¹⁶, and the resulting pump sequence is described by the following elliptic path in parameter space: $(J_1 - J_2)/a^2 + (\Delta/b)^2 = 1$, with $a \approx 0.19 E_R$ and $b \approx 0.475 E_R$. In our numerics, we choose a closely related pumping sequence with $a = 0.15 E_R$ and $b = 0.5 E_R$; this choice does not affect our final conclusions, since topological pumping is robust against smooth deformations of the pumping sequence. Finally, to reveal the interaction-induced topological transport for impurities, we propose to implement a trivial pump sequence for that species only [see Fig. 5]; this could be realized by designing a state-dependent optical lattice⁶⁰, for instance, using the Floquet-engineering scheme of ref. 61.

The particle numbers of the two species can be set to $N_\phi \approx 1500$ ⁶² and $N_\sigma/N_\phi \approx 1/30$. With this choice, we obtain the interaction parameters according to the relation $g_{\alpha\beta}/E_R = (N_\sigma + N_\phi) \sqrt{8/\pi} k_l a_{\alpha\beta}(V_s/E_R)^{3/4}$ ⁴⁰, where $\alpha, \beta = (\phi, \sigma)$ and $k_l = 2\pi/\lambda_l$. Setting the pump parameter $J_0 = 0.5 E_R$, the numerical values for the interaction parameters are obtained as $g_{\phi\phi} \approx 0.226 J_0$, $g_{\phi\sigma} \approx -11.32 J_0$ and $g_{\sigma\sigma} \approx 2.26 J_0$, which are the values used in our numerical simulations [Fig. 5].

Discussion

In this work, we outlined a general theoretical framework that connects Bloch band's topology to nonlinear excitations, hence elucidating the topological transport of solitons in the context of nonlinear Thouless pumps. Solitons are stable states of nonlinear lattice systems described by the paradigmatic discrete nonlinear Schrödinger equation (DNLS), which is central in describing nonlinear phenomena in a wide range of physical settings, from nonlinear optics and photonics, to ultracold

quantum matter, fluid dynamics and plasma physics. In this sense, characterizing the influence of Bloch band's topology on the behavior of the stable states of DNLS is of prime importance. This program is particularly challenging due to the lack of generic theoretical approaches connecting notions of topological physics to nonlinear systems and vice versa. Furthermore, introducing nonlinearities in more sophisticated topological systems, such as higher-dimensional settings, or lattices exhibiting higher-order topology and symmetry-protected features, could lead to exotic phenomena exhibited by the nonlinear modes of the system; see ref. 63 and references therein. By providing a scheme that naturally connects topological indices of band structures to nonlinear excitations, our work opens the door to the exploration of novel nonlinear topological phenomena.

We also illustrated the universality of our approach, by introducing a topological pump for Bose-Bose atomic mixtures, where one species (impurity atoms) experience a quantized drift through genuine interaction processes with the other species (the surrounding majority atoms). Importantly, the impurity atoms inherit the topological properties of their environment through inter-species interactions. We note that such interaction-induced topology has been previously studied in the context of topological polarons, namely, in mixtures with strong population imbalance, where individual topological excitations can bind to mobile impurities^{50,51,53,55}. The present scheme extends those concepts to more complex majority-impurity states, such as coupled coherent states within a superfluid phase. We also point out that the proposed scheme can be implemented using available cold-atom technologies, and the quantized transport of impurities can be measured in-situ, using state-selective imaging techniques⁶⁴. Besides, the Chern number characterizing the interaction-induced topological pump could also be directly extracted by interferometry⁵¹.

During the preparation of this manuscript, the authors became aware of a related work by M. Jürgensen and M. C. Rechtsman⁴⁷, and also ref. 65.

Methods

Adiabatic theorem for NLS

The adiabatic theorem for NLS (both continuous and discrete forms), follows closely the formulation of its linear counterpart^{43,44}. For a system with a time-dependent Hamiltonian $H(t)$, which varies on a time scale T much larger than all the time scales in the problem, the time-dependent NLS takes the following form (see main text)

$$i\varepsilon \partial_s \phi = H(s) \phi - g|\phi|^2 \phi, \quad (13)$$

where $s = t/T$ is the adiabatic time and $\varepsilon = 1/T$ the rate of change. The stationary state solutions of Eq. (13) are of the form

$$\phi_s = e^{-i\theta_s} (\varphi_s + \delta \varphi_s), \quad (14)$$

where φ_s is the instantaneous solution of the stationary NLS,

$$\mu_s \varphi_s = H(s) \varphi_s - g|\varphi_s|^2 \varphi_s, \quad (15)$$

and $\theta_s = 1/\varepsilon (\int_0^s ds' \mu_{s'} - \gamma_s)$ is a global phase factor consisting of a dynamical contribution and a Berry phase, and it can be ignored. The correction term $\delta \varphi_s$ accounts for non-adiabatic variations, and for $\varepsilon \rightarrow 0$, it behaves as $\|\delta \varphi\| \sim \varepsilon$, hence vanishes in the adiabatic limit $\varepsilon \rightarrow 0$. The relevant dynamical information is therefore encoded in the instantaneous solutions of Eq. (15).

The Rice-Mele model and pump sequence

Throughout this work, we illustrate the general concepts and results using the Rice-Mele model, with periodic boundary conditions. This simple two-band model, which is reviewed in some detail below, is known to exhibit a topological (Thouless) pump sequence.

The Rice-Mele model is a 1D tight-binding model with alternating nearest-neighbor tunneling matrix elements ($J_1, J_2, J_1, J_2, \dots$), and a staggered on-site potential. We denote the two sites within each unit cell by $\alpha = A, B$ and the unit cells by $i, 0 \leq i \leq N-1$, where N is the number of unit cells. The hopping matrix element between sites A and B within each unit cell (resp. between adjacent unit cells) is written as $J_1 = -J(1 + \delta)$ (resp. $J_2 = -J(1 - \delta)$) and the magnitude of the staggered potential on site A (resp. B) equals Δ (resp. $-\Delta$). The Hamiltonian of the Rice-Mele model thus reads

$$H = - \sum_{i=0}^{N-1} [J(1 + \delta) |i, A\rangle \langle i, B| + J(1 - \delta) |i, A\rangle \langle i - 1, B|]$$
(16)

$$+ \frac{\Delta}{2} \sum_{i=0}^{N-1} [|i, A\rangle \langle i, A| - |i, B\rangle \langle i, B|] + \text{h.c.}$$
(17)

The simulations shown in the main text were performed on a lattice with $N = 100$ unit cells, and using the following pump sequence

$$\begin{aligned} J(s) &= J_0 (1 + 1/2 \cos(2\pi s)), \\ \delta(s) &= \delta_0 \cos(2\pi s) / (2 + \cos(2\pi s)), \\ \Delta(s) &= J_0 \sin(2\pi s), \end{aligned}$$
(18)

with $J_0 = 0.5$ and $\delta_0 = 0.6$, corresponding to a topological pump with Chern number $C = -1$. The *nonlinear* Rice-Mele model, which is used in our simulations, is obtained by adding an on-site nonlinearity to this lattice model; see Eq. (2).

In order to demonstrate the interaction-induced topological pumping in the Bose-Bose mixture setting, we assume that the two species experience the same Rice-Mele lattice described above, but with different pump sequences: the majority atoms experience the topological pumping sequence in Eq. (18), while the impurity atoms experience a trivial sequence with $J\delta = \Delta = 0$. The resulting center-of-mass displacement of both species are depicted in Fig. 5 of the main text.

Derivation of the scalar DNLS

We outline the derivation of the simplified scalar DNLS from the original lattice DNLS,

$$\mu \phi_i = \sum_j H_{ij} \phi_j - g |\phi_i|^2 \phi_i.$$
(19)

The Wannier functions are related to the Bloch waves of the Hamiltonian by the following relations:

$$\begin{aligned} w_j^{(n)}(l) &= \frac{1}{\sqrt{N}} \sum_{k=0}^{N-1} e^{i(2\pi/N)k(l-j)} \psi_j^{(n)}(k) \\ &= \frac{1}{\sqrt{N}} \sum_{k=0}^{N-1} e^{i(2\pi/N)k(j-l)} u_j^{(n)}(k), \end{aligned}$$
(20)

where $\psi_j^{(n)}(k) = e^{i(2\pi/N)kj} u_j^{(n)}(k)$ is the Bloch wave of band n with momentum k and $u_j^{(n)}(k)$ is the corresponding Bloch function, which is periodic over the unit cells and does not depend on j . To represent the Hamiltonian part in Wannier basis, we evaluate the matrix elements of the Hamiltonian over the Wannier states

$$\begin{aligned} \langle w^{(n)}(l'), H w^{(n)}(l) \rangle &= \frac{1}{N} \sum_{k, k'=0}^{N-1} e^{i(2\pi/N)(k'l - kl)} \langle \psi^{(n)}(k'), H \psi^{(n)}(k) \rangle \\ &= \delta_{nn'} \cdot \frac{1}{N} \sum_{k=0}^{N-1} e^{i(2\pi/N)k(l'-l)} \epsilon_k^{(n)} = \delta_{nn'} \cdot \omega_{l'-l}^{(n)}, \end{aligned}$$
(21)

where $\omega_l^{(n)} = 1/N \sum_{k=0}^{N-1} e^{i(2\pi/N)kl} \epsilon_k^{(n)}$ is the Fourier transform of the Bloch band $\epsilon_k^{(n)}$; see main text.

Next, we express the nonlinearity in terms of Wannier functions,

$$\begin{aligned} \langle w^{(n)}(l), |\phi|^2 \phi \rangle &= \sum_{n_1, n_2, n_3} \sum_{l_1, l_2, l_3} \left(\sum_i w_i^{(n_1)*}(l) w_i^{(n_1)}(l_1) w_i^{(n_2)}(l_2) w_i^{(n_3)}(l_3) \right) \\ &\times a_{l_1}^{(n_1)*} a_{l_2}^{(n_2)} a_{l_3}^{(n_3)}. \end{aligned}$$
(22)

Taking the inner product of Eq. (19) with $w_l^{(n)}$ and using Eqs. (21) and (22), we obtain the following DNLS

$$\begin{aligned} \mu_s a_l^{(n)} &= \sum_{l_1} \omega_{l-l_1}^{(n)} a_{l_1}^{(n)} \\ &- g \sum_{n_1, n_2, n_3} \sum_{l_1, l_2, l_3} W_{l-l_1}^{(n)} a_{l_1}^{(n_1)*} a_{l_2}^{(n_2)} a_{l_3}^{(n_3)}. \end{aligned}$$
(23)

Derivation of the soliton center-of-mass displacement

Here, we prove that the quantized displacement of the solitons center-of-mass is determined by the Chern number of the related Bloch band. For later convenience, we derive the following identity for matrix elements of position operator over the Wannier functions,

$$\begin{aligned} \langle w^{(n)}(l'), X w^{(n)}(l) \rangle &= \langle w^{(n)}(l' - l), (T_l^\dagger X T_l) w^{(n)}(0) \rangle \\ &= \langle w^{(n)}(l' - l), X w^{(n)}(0) \rangle + l \langle w^{(n)}(l' - l), w^{(n)}(0) \rangle \\ &= \langle w^{(n)}(l' - l), X w^{(n)}(0) \rangle + l \delta_{ll'}. \end{aligned}$$
(24)

where T_l is the translation operator by l unit cells. In deriving Eq. (24) we used the relation $T_l^\dagger X T_l = X + l$ together with the orthogonality of Wannier functions. The soliton center-of-mass then reads

$$\begin{aligned} \langle \varphi^{(n)}, X \varphi^{(n)} \rangle_s &= \sum_{l, l'} a_l^{(n)*} a_{l'}^{(n)} \langle w^{(n)}(l'), X w^{(n)}(l) \rangle_s \\ &= \sum_l |a_l^{(n)}|^2 \langle w^{(n)}(l), X w^{(n)}(l) \rangle_s \\ &+ \sum_{l \neq l'} a_l^{(n)*} a_{l'}^{(n)} \langle w^{(n)}(l'), X w^{(n)}(l) \rangle_s \\ &= \left(\sum_l |a_l^{(n)}|^2 \right) \langle w^{(n)}(0), X w^{(n)}(0) \rangle_s \\ &+ \left(\sum_l |a_l^{(n)}|^2 l \right) \langle w^{(n)}(0), w^{(n)}(0) \rangle_s \\ &+ \sum_{\delta \neq 0} \left(\sum_l a_{l+\delta}^{(n)*} a_l^{(n)} \right) \langle w^{(n)}(\delta l), X w^{(n)}(0) \rangle_s, \end{aligned}$$
(25)

where we used Eq. (24) in the last equality. The first term in the last equality of Eq. (25) reduces to $\langle w^{(n)}(0), X w^{(n)}(0) \rangle_s$ since we normalized the soliton intensity to unity, $N_\phi = \sum_l |a_l^{(n)}|^2 = 1$. The second term in the last expression is the mean value of the position of the Wannier functions indices, which is constant since the on-site solution is always peaked around a Wannier label and remains symmetric around it. Its contribution to the displacement over a pump cycle thus vanishes. The third term contains products of the form $\left(\sum_l a_{l+\delta l}^{(n)*} a_l^{(n)} \right) \langle w^{(n)}(\delta l), X w^{(n)}(0) \rangle_s$ and its treatment requires more care. The coefficient $\left(\sum_l a_{l+\delta l}^{(n)*} a_l^{(n)} \right)$ is time-periodic, since $a_l^{(n)}$ is, by assumption, the solution of the scalar DNLS in Eq. (7), in the main text. To investigate the behavior of $\langle w^{(n)}(\delta l), X w^{(n)}(0) \rangle_s$, we note that after a pump cycle, the Wannier functions are displaced by the Chern number, $w^{(n)}(l)|_{s=1} = w^{(n)}(l + C_n)|_{s=0}$, with C_n the Chern number of

band n . Thus, after a pump cycle, we have

$$\begin{aligned} \langle w^{(n)}(\delta l), Xw^{(n)}(0) \rangle|_{s=1} & \\ = \langle w^{(n)}(\delta l + C_n), Xw^{(n)}(C_n) \rangle|_{s=0} & \quad (26) \\ = \langle w^{(n)}(\delta l), Xw^{(n)}(0) \rangle|_{s=0}. & \end{aligned}$$

where we used Eq. (24) in the last step. This proves that the quantity $\langle w^{(n)}(\delta l), Xw^{(n)}(0) \rangle|_s$, in the last equality of Eq. (25), is a time-periodic quantity.

Altogether, the third term in Eq. (25) is also time-periodic, and the soliton's center-of-mass displacement over a pump cycle is given by

$$\Delta \langle \varphi^{(n)}, X\varphi^{(n)} \rangle = \Delta \langle w^{(n)}(0), Xw^{(n)}(0) \rangle. \quad (27)$$

This result directly relates the soliton's displacement to the displacement of Wannier functions upon one pump cycle, as dictated by the Chern number of the band^{15,38,39}. This proves the quantized pumping of the soliton according to the Chern number.

Derivation of the Bose-Bose mixture equations

In order to derive the equations governing the coherent state profiles of the two species in the mixture, we start from the microscopic Hamiltonian in Eq. (9). The coherent-state action of the system takes the following form ($\hbar = 1$),

$$S[\bar{\phi}, \phi; \bar{\sigma}, \sigma] = \int_{t_i}^{t_f} dt L[\bar{\phi}, \phi; \bar{\sigma}, \sigma], \quad (28)$$

with the Lagrangian

$$\begin{aligned} L[\bar{\phi}, \phi; \bar{\sigma}, \sigma] & \\ = \sum_{\mathbf{i}} \bar{\phi}_{\mathbf{i}} [i\partial_t + \mu_{\phi}] \phi_{\mathbf{i}} - \sum_{\langle \mathbf{i}, \mathbf{j} \rangle} \bar{\phi}_{\mathbf{i}} t_{\phi} H_{\mathbf{ij}}^{(\phi)} \phi_{\mathbf{j}} - \sum_{\mathbf{i}} \frac{g_{\phi\phi}}{2} |\phi_{\mathbf{i}}|^4 & \\ + \sum_{\mathbf{i}} \bar{\sigma}_{\mathbf{i}} [i\partial_t + \mu_{\sigma}] \sigma_{\mathbf{i}} - \sum_{\langle \mathbf{i}, \mathbf{j} \rangle} \bar{\sigma}_{\mathbf{i}} H_{\mathbf{ij}}^{(\sigma)} \sigma_{\mathbf{j}} - \sum_{\mathbf{i}} \frac{g_{\sigma\sigma}}{2} |\sigma_{\mathbf{i}}|^4 & \quad (29) \\ - \sum_{\mathbf{i}} g_{\phi\sigma} |\sigma_{\mathbf{i}}|^2 |\phi_{\mathbf{i}}|^2. & \end{aligned}$$

To proceed, we seek stationary state solutions for the coherent state fields of the form $\phi_{\mathbf{i}}^{(ss)}(t) = e^{-i\omega_{\phi} t} \phi_{\mathbf{i}}$ and $\sigma_{\mathbf{i}}^{(ss)}(t) = e^{-i\omega_{\sigma} t} \sigma_{\mathbf{i}}$, which minimize $L[\bar{\phi}, \phi; \bar{\sigma}, \sigma]$. Such solutions are the saddle-point solutions of the quantum mechanical action, giving the mean-field stable states of the system. The Lagrangian then takes the time-independent form

$$\begin{aligned} L[\bar{\phi}, \phi; \bar{\sigma}, \sigma] & \\ = \sum_{\mathbf{i}} \bar{\phi}_{\mathbf{i}} [\omega_{\phi} + \mu_{\phi}] \phi_{\mathbf{i}} - \sum_{\langle \mathbf{i}, \mathbf{j} \rangle} \bar{\phi}_{\mathbf{i}} H_{\mathbf{ij}}^{(\phi)} \phi_{\mathbf{j}} - \sum_{\mathbf{i}} \frac{g_{\phi\phi}}{2} |\phi_{\mathbf{i}}|^4 & \\ + \sum_{\mathbf{i}} \bar{\sigma}_{\mathbf{i}} [\omega_{\sigma} + \mu_{\sigma}] \sigma_{\mathbf{i}} - \sum_{\langle \mathbf{i}, \mathbf{j} \rangle} \bar{\sigma}_{\mathbf{i}} H_{\mathbf{ij}}^{(\sigma)} \sigma_{\mathbf{j}} - \sum_{\mathbf{i}} \frac{g_{\sigma\sigma}}{2} |\sigma_{\mathbf{i}}|^4 & \quad (30) \\ - \sum_{\mathbf{i}} g_{\phi\sigma} |\sigma_{\mathbf{i}}|^2 |\phi_{\mathbf{i}}|^2. & \end{aligned}$$

To minimize the Lagrangian, the corresponding Euler-Lagrange equations are derived from $\delta L / \delta \bar{\phi}_{\mathbf{i}} = 0$ and $\delta L / \delta \bar{\sigma}_{\mathbf{i}} = 0$, which leads to the two coupled equations in Eq. (10) in the main text.

In the limiting case of heavy impurities, we neglect their kinetic energy contributions ($H_{\mathbf{ij}}^{(\sigma)}$) to Eq. (10), the so-called Thomas-Fermi approximation. In this case, the second equation in Eq. (10) reduces to $(\omega_{\sigma} + \mu_{\sigma}) = g_{\phi\sigma} |\phi_{\mathbf{i}}|^2 + g_{\sigma\sigma} |\sigma_{\mathbf{i}}|^2$. For the bright soliton solutions of Eq. (10), $\phi_{\mathbf{i}}$ and $\sigma_{\mathbf{i}}$ decay exponentially away from the soliton center, thus, to zeroth order in the impurities hopping strength, $\omega_{\sigma} + \mu_{\sigma} = 0$. Eq. (10)

then reduce to

$$(\omega_{\phi} + \mu_{\phi}) \phi_{\mathbf{i}} = \sum_{\mathbf{j}} H_{\mathbf{ij}}^{(\phi)} \phi_{\mathbf{j}} + (g_{\phi\phi} |\phi_{\mathbf{i}}|^2 + g_{\phi\sigma} |\sigma_{\mathbf{i}}|^2) \phi_{\mathbf{i}}, \quad (31)$$

$$|\sigma_{\mathbf{i}}|^2 = -g_{\phi\sigma} / g_{\sigma\sigma} |\phi_{\mathbf{i}}|^2. \quad (32)$$

Inserting Eq. (32) into Eq. (31), we obtain an effective DNLS for $\phi_{\mathbf{i}}$,

$$(\omega_{\phi} + \mu_{\phi}) \phi_{\mathbf{i}} = \sum_{\mathbf{j}} H_{\mathbf{ij}}^{(\phi)} \phi_{\mathbf{j}} + (g_{\phi\phi} - g_{\phi\sigma}^2 / g_{\sigma\sigma}) |\phi_{\mathbf{i}}|^2 \phi_{\mathbf{i}}, \quad (33)$$

with the effective nonlinearity strength $g = -g_{\phi\phi} + g_{\phi\sigma}^2 / g_{\sigma\sigma}$, which for $g_{\phi\phi} g_{\sigma\sigma} < g_{\phi\sigma}^2$ corresponds to a defocusing nonlinearity.

Variational ansatz for the state of Bose-Bose mixture in the Thomas-Fermi limit

The variational treatment of Eqs. (11) and (12) accounts to minimizing the following energy functional for the field ϕ

$$\begin{aligned} H[\bar{\phi}, \phi] = \sum_{\mathbf{i}, \mathbf{j}} \bar{\phi}_{\mathbf{i}} H_{\mathbf{ij}}^{(\phi)} \phi_{\mathbf{j}} - \frac{g}{2} \sum_{\mathbf{i}} |\phi_{\mathbf{i}}|^2 & \\ - \mu_{\phi} \left(\sum_{\mathbf{i}} |\phi_{\mathbf{i}}|^2 - N_{\phi} \right). & \quad (34) \end{aligned}$$

From the knowledge obtained from the soliton solutions of the DNLS in the main text, we assume that $\phi_{\mathbf{i}}$ belongs to a single band and expand it in terms of the Wannier functions of the corresponding band, $\phi_{\mathbf{i}} = \sum_l a_l^{(n)} w^{(n)}(l)$. We then use a sech variational ansatz for the coefficient amplitudes, $a_l^{(n)} = \eta / \text{sech}(\xi(l - l_0))$. The variational energy functional takes the following form:

$$\begin{aligned} H / \eta^2 = \omega_0^{(n)} N_{\phi} / \eta^2 + \sum_{m=1}^{\infty} \frac{4m}{\sinh(\xi m)} \omega_m^{(n)} & \\ - \frac{2gW^{(n)}}{3} \eta^2 \left[\frac{1}{\xi} + \sum_{m=1}^{\infty} \frac{2\pi^2}{\xi^2} \left(1 + \frac{\pi^2 m^2}{\xi^2} \right) \frac{m \cos(2\pi m l_0)}{\sinh(\frac{\pi^2 m}{\xi})} \right], & \quad (35) \end{aligned}$$

subject to the constraint $N_{\phi} = \text{const.}$, where

$$N_{\phi} / \eta^2 = \frac{2}{\xi} + \sum_{m=1}^{\infty} \frac{4\pi^2 m \cos(2\pi m l_0)}{\xi^2 \sinh(\frac{\pi^2 m}{\xi})}. \quad (36)$$

For the simulations presented in the main text [Fig. 4], we assume that $N_{\phi} = 1$; see refs. 36, 48 for more details on variational ansätze for DNLS. From the solution of Eqs. (35) and (36) we then obtain the boson field, $\phi_{\mathbf{i}}$, which is then used to obtain the effective attractive potential $u_{\mathbf{i}}^{\text{MF}} = g |\phi_{\mathbf{i}}|^2$; see Eq. (12).

Potential barrier preventing soliton delocalization

The nonlinear term in Eq. (1) [resp. in Eq. (7)] leads to the formation of localized soliton solutions, which do not satisfy the lattice (resp. Wannier lattice) translational symmetry. While the stable-state solitons are not translationally invariant, they can be mapped to one another through lattice translations. It is known that an effective potential barrier exists for continuous deformations of each stable-state soliton to a neighboring one. This potential barrier is reminiscent of the Peierls-Naborro barrier (PNB) known in the theory of dislocation dynamics in crystals⁶⁶. Under adiabatic evolution, a soliton in Wannier representation will always remain peaked on a single Wannier index since the potential barrier rules out the existence of solutions that interpolate continuously between two on-site solitons. The strength of this potential barrier can be estimated in terms of the model

parameters using the variational ansatz $a_l^{(n)} = \eta / \text{sech}(\xi(l - l_0))$ for the Wannier soliton in band n , and the corresponding energy functional in Eq. (35),

$$\begin{aligned} \Delta_{\text{Barrier}} &\simeq H(\eta_0, \xi_0, l_0 = 1/2) - H(\eta_0, \xi_0, l_0 = 0) \\ &\simeq \sum_{m=1}^{\infty} \left[\frac{4\pi^2 \omega_0^{(n)} \eta_0^2}{\xi_0^2} - \frac{4\pi^2 g}{3\xi_0^2} \eta_0^4 \left(1 + \frac{\pi^2 m^2}{\xi_0^2} \right) \right] \\ &\quad \times \frac{m(1 - (-1)^m)}{\sinh\left(\frac{\pi^2 m}{\xi_0}\right)}, \end{aligned} \quad (37)$$

where

$$H(\eta_0, \xi_0, l_0 = 0) = \min_{\eta, \xi} H(\eta, \xi, l_0 = 0). \quad (38)$$

The estimated Δ_{Barrier} depends on the model parameters via the Fourier transform of the dispersion relation at $l=0$, $\omega_0^{(n)} = 1/N \sum_{k=0}^{N-1} \epsilon_k^{(n)}$, and the interaction parameter g . We verified that the expression in Eq. (37) is in agreement with a result found in ref. 36 for DNLS equations with nearest-neighbor hopping.

Data availability

The data that support the findings of this study are available from the corresponding author upon reasonable request.

Code availability

The code that supports the plots within this paper are available from the corresponding author upon reasonable request.

References

- Hasan, M. Z. & Kane, C. L. Colloquium: topological insulators. *Rev. Mod. Phys.* **82**, 3045–3067 (2010).
- Qi, X.-L. & Zhang, S.-C. Topological insulators and superconductors. *Rev. Mod. Phys.* **83**, 1057–1110 (2011).
- Wu, L. et al. Quantized Faraday and Kerr rotation and axion electrodynamics of a 3d topological insulator. *Science* **354**, 1124–1127 (2016).
- Asteria, L. et al. Measuring quantized circular dichroism in ultracold topological matter. *Nat. Phys.* **15**, 449–454 (2019).
- Li, T. et al. Bloch state tomography using Wilson lines. *Science* **352**, 1094–1097 (2016).
- Hoeller, J. & Alexandradinata, A. Topological Bloch oscillations. *Phys. Rev. B* **98**, 024310 (2018).
- Thouless, D. J. Quantization of particle transport. *Phys. Rev. B* **27**, 6083–6087 (1983).
- Xiao, D., Chang, M.-C. & Niu, Q. Berry phase effects on electronic properties. *Rev. Mod. Phys.* **82**, 1959–2007 (2010).
- Kraus, Y. E., Lahini, Y., Ringel, Z., Verbin, M. & Zilberberg, O. Topological states and adiabatic pumping in quasicrystals. *Phys. Rev. Lett.* **109**, 106402 (2012).
- Verbin, M., Zilberberg, O., Lahini, Y., Kraus, Y. E. & Silberberg, Y. Topological pumping over a photonic fibonacci quasicrystal. *Phys. Rev. B* **91**, 064201 (2015).
- Zilberberg, O. et al. Photonic topological boundary pumping as a probe of 4d quantum hall physics. *Nature* **553**, 59–62 (2018).
- Grinberg, I. H. et al. Robust temporal pumping in a magneto-mechanical topological insulator. *Nat. Commun.* **11**, 1–9 (2020).
- Cerjan, A., Wang, M., Huang, S., Chen, K. P. & Rechtsman, M. C. Thouless pumping in disordered photonic systems. *Light Sci. Appl.* **9**, 1–7 (2020).
- Ke, Y. et al. Topological phase transitions and Thouless pumping of light in photonic waveguide arrays. *Laser Photon. Rev.* **10**, 995–1001 (2016).
- Lohse, M., Schweizer, C., Zilberberg, O., Aidelsburger, M. & Bloch, I. A Thouless quantum pump with ultracold bosonic atoms in an optical superlattice. *Nat. Phys.* **12**, 350–354 (2016).
- Nakajima, S. et al. Topological Thouless pumping of ultracold fermions. *Nat. Phys.* **12**, 296–300 (2016).
- Ozawa, T. et al. Topological photonics. *Rev. Mod. Phys.* **91**, 015006 (2019).
- Cooper, N., Dalibard, J. & Spielman, I. Topological bands for ultracold atoms. *Rev. Mod. Phys.* **91**, 015005 (2019).
- Smirnova, D., Leykam, D., Chong, Y. & Kivshar, Y. Nonlinear topological photonics. *Appl. Phys. Rev.* **7**, 021306 (2020).
- Leykam, D. & Chong, Y. D. Edge solitons in nonlinear-photonic topological insulators. *Phys. Rev. Lett.* **117**, 143901 (2016).
- Solnyshkov, D., Bleu, O., Teklu, B. & Malpuech, G. Chirality of topological gap solitons in bosonic dimer chains. *Phys. Rev. Lett.* **118**, 023901 (2017).
- St-Jean, P. et al. Lasing in topological edge states of a one-dimensional lattice. *Nat. Photon.* **11**, 651–656 (2017).
- Bisianov, A., Wimmer, M., Peschel, U. & Egorov, O. Stability of topologically protected edge states in nonlinear fiber loops. *Physical Review A* **100**, 063830 (2019).
- Ivanov, S. K., Kartashov, Y. V., Szameit, A., Torner, L. & Konotop, V. V. Vector topological edge solitons in Floquet insulators. *ACS Photon.* **7**, 735–745 (2020).
- González-Cuadra, D., Dauphin, A., Grzybowski, P. R., Lewenstein, M. & Bermudez, A. Dynamical solitons and boson fractionalization in cold-atom topological insulators. *Phys. Rev. Lett.* **125**, 265301 (2020).
- Mukherjee, S. & Rechtsman, M. C. Observation of Floquet solitons in a topological bandgap. *Science* **368**, 856–859 (2020).
- Mukherjee, S. & Rechtsman, M. C. Observation of unidirectional solitonlike edge states in nonlinear Floquet topological insulators. *Phys. Rev. X*, 041057 (2021).
- Xia, S. et al. Nontrivial coupling of light into a defect: the interplay of nonlinearity and topology. *Light: Sci. Appl.* **9**, 1–10 (2020).
- Pernet, N. et al. Gap solitons in a one-dimensional driven-dissipative topological lattice. *Nat. Phys.* **18**, 678–684 (2022).
- Mittal, S. et al. Topological frequency combs and nested temporal solitons. *Nat. Phys.* **17**, 1169–1176 (2021).
- Kirsch, M. S. et al. Nonlinear second-order photonic topological insulators. *Nat. Phys.* **17**, 995–1000 (2021).
- Lo, P.-W. et al. Topology in nonlinear mechanical systems. *Phys. Rev. Lett.* **127**, 076802 (2021).
- Oblak, B. & Kozyreff, G. Berry phases in the reconstructed KDV equation. *Chaos: An Interdisciplinary. J. Nonlinear Sci.* **30**, 113114 (2020).
- Jürgensen, M., Mukherjee, S. & Rechtsman, M. C. Quantized nonlinear Thouless pumping. *Nature* **596**, 63–67 (2021).
- Sulem, C. & Sulem, P. *The Nonlinear Schrödinger Equation*. (Springer-Verlag, New York, 1999).
- Kevrekidis, P. G. *The Discrete Nonlinear Schrödinger Equation: Mathematical Analysis, Numerical Computations and Physical Perspectives* vol. 232 (Springer Science & Business Media, 2009).
- Alfimov, G., Kevrekidis, P., Konotop, V. & Salerno, M. Wannier functions analysis of the nonlinear Schrödinger equation with a periodic potential. *Physical Review E* **66**, 046608 (2002).
- Asbóth, J. K., Oroszlány, L. & Pályi, A. A short course on topological insulators. *Lect. Notes Phys.* **919**, 166 (2016).
- Mei, F. et al. Topological insulator and particle pumping in a one-dimensional shaken optical lattice. *Phys. Rev. A* **90**, 063638 (2014).
- Bloch, I., Dalibard, J. & Zwirger, W. Many-body physics with ultracold gases. *Rev. Mod. Phys.* **80**, 885–964 (2008).
- Chin, C., Grimm, R., Julienne, P. & Tiesinga, E. Feshbach resonances in ultracold gases. *Rev. Mod. Phys.* **82**, 1225–1286 (2010).

42. Sowinski, T. & Garcia-March, M. A. One-dimensional mixtures of several ultracold atoms: a review. *Rep. Prog. Phys.* **82**, 104401 (2019).
43. Gang, Z. & Grech, P. Adiabatic theorem for the Gross-Pitaevskii equation. *Commun. Part. Differ. Equ.* **42**, 731–756 (2017).
44. Carles, R. & Sparber, C. Semiclassical wave packet dynamics in Schrödinger equations with periodic potentials. *Discr. Contin. Dyn. Syst. -Ser. B* **17**(3), 759–774 (2012).
45. Szameit, A. & Nolte, S. Discrete optics in femtosecond-laser-written photonic structures. *J. Phys. B: Atom. Mol. Opt. Phys.* **43**, 163001 (2010).
46. Yu, R., Qi, X. L., Bernevig, A., Fang, Z. & Dai, X. Equivalent expression of Z2 topological invariant for band insulators using the non-Abelian Berry connection. *Phys. Rev. B* **84**, 075119 (2011).
47. Jürgensen, M. & Rechtsman, M. C. The Chern number governs soliton motion in nonlinear Thouless pumps. *Phys. Rev. Lett.* **128**, 113901 (2022).
48. Kevrekidis, P. G., Kivshar, Y. S. & Kovalev, A. S. Instabilities and bifurcations of nonlinear impurity modes. *Phys. Rev. E* **67**, 046604 (2003).
49. Kivshar, Y. S. & Campbell, D. K. Peierls-Nabarro potential barrier for highly localized nonlinear modes. *Phys. Rev. E* **48**, 3077–3081 (1993).
50. Grusdt, F., Yao, N. Y., Abanin, D., Fleischhauer, M. & Demler, E. Interferometric measurements of many-body topological invariants using mobile impurities. *Nat. Commun.* **7**, 1–9 (2016).
51. Grusdt, F., Yao, N. Y. & Demler, E. Topological polarons, quasi-particle invariants, and their detection in one-dimensional symmetry-protected phases. *Phys. Rev. B* **100**, 075126 (2019).
52. Camacho-Guardian, A., Goldman, N., Massignan, P. & Bruun, G. M. Dropping an impurity into a chern insulator: A polaron view on topological matter. *Phys. Rev. B* **99**, 081105 (2019).
53. Heras, A. M., Macaluso, E. & Carusotto, I. Anyonic molecules in atomic fractional quantum Hall liquids: a quantitative probe of fractional charge and anyonic statistics. *Phys. Rev. X* **10**, 041058 (2020). de las.
54. Pimenov, D. et al. Topological transport of mobile impurities. *Phys. Rev. B* **103**, 245106 (2021).
55. Baldelli, N., Juliá-Díaz, B., Bhattacharya, U., Lewenstein, M. & Graß, T. Tracing non-Abelian anyons via impurity particles. *Phys. Rev. B* **104**, 035133 (2021).
56. Grusdt, F. & Demler, E. New theoretical approaches to Bose polarons. *Quantum Matter Ultralow Temp.* **191**, 325–404 (2015).
57. Strecker, K. E., Partridge, G. B., Truscott, A. G. & Hulet, R. G. Formation and propagation of matter-wave soliton trains. *Nature* **417**, 150–153 (2002).
58. Ahufinger, V., Sanpera, A., Pedri, P., Santos, L. & Lewenstein, M. Creation and mobility of discrete solitons in Bose-Einstein condensates. *Phys. Rev. A* **69**, 053604 (2004).
59. Hulet, R. G., Nguyen, J. H. V. & Senaratne, R. Methods for preparing quantum gases of lithium. *Rev. Sci. Instrum.* **91**, 011101 (2020).
60. Jaksch, D. & Zoller, P. The cold atom Hubbard toolbox. *Ann. Phys.* **315**, 52–79 (2005).
61. Jotzu, G. et al. Creating state-dependent lattices for ultracold fermions by magnetic gradient modulation. *Phys. Rev. Lett.* **115**, 073002 (2015).
62. Bradley, C. C., Sackett, C. A. & Hulet, R. G. Bose-Einstein condensation of lithium: Observation of limited condensate number. *Phys. Rev. Lett.* **78**, 985–989 (1997).
63. Di Liberto, M. & Goldman, N. Orbital order and chiral currents of interacting bosons with π -flux. Preprint at <https://arxiv.org/pdf/2111.13572.pdf> (2021).
64. Bloch, I., Dalibard, J. & Nascimbene, S. Quantum simulations with ultracold quantum gases. *Nat. Phys.* **8**, 267–276 (2012).
65. Fu, Q., Wang, P., Kartashov, Y. V., Konotop, V. V. & Ye, F. Nonlinear Thouless pumping: solitons and transport breakdown. *Phys. Rev. Lett.* **128**, 154101 (2022).
66. Anderson, P. M., Hirth, J. P. & Lothe, J. *Theory of dislocations* (Cambridge University Press, 2017).

Acknowledgements

We are glad to thank B. Oblak, A. Bedroja, N. Englebort, S.-P. Gorza, F. Leo and S. Mukherjee for useful discussions. We also acknowledge M. Jürgensen and M. C. Rechtsman for fruitful discussions, for sharing their results in the course of our numerical studies and for enlightening us on the negligible role of band mixing. N.G. is supported by the FRS-FNRS (Belgium) and the ERC Starting Grant TopoCold. N.M. and F.G. acknowledge funding by the Deutsche Forschungsgemeinschaft (DFG, German Research Foundation) under Germany's Excellence Strategy-EXC-2111-390814868 and via Research Unit FOR 2414 under project number 277974659.

Author contributions

N.M. conceived the theoretical framework under the supervision of N.G., with inputs from F.G.. N.M. performed the analytic calculations and numerical simulations, with inputs from N.G.. All authors analyzed and discussed the results. N.M. and N.G. wrote the manuscript with inputs from F.G..

Competing interests

The authors declare no competing interests.

Additional information

Correspondence and requests for materials should be addressed to Nader Mostaan or Nathan Goldman.

Peer review information *Nature Communications* thanks Mohammad Hafezi and the other, anonymous, reviewer(s) for their contribution to the peer review of this work.

Reprints and permission information is available at

<http://www.nature.com/reprints>

Publisher's note Springer Nature remains neutral with regard to jurisdictional claims in published maps and institutional affiliations.

Open Access This article is licensed under a Creative Commons Attribution 4.0 International License, which permits use, sharing, adaptation, distribution and reproduction in any medium or format, as long as you give appropriate credit to the original author(s) and the source, provide a link to the Creative Commons license, and indicate if changes were made. The images or other third party material in this article are included in the article's Creative Commons license, unless indicated otherwise in a credit line to the material. If material is not included in the article's Creative Commons license and your intended use is not permitted by statutory regulation or exceeds the permitted use, you will need to obtain permission directly from the copyright holder. To view a copy of this license, visit <http://creativecommons.org/licenses/by/4.0/>.

© The Author(s) 2022, corrected publication 2022